JACS
JOURNAL OF THE AMERICAN CHEMICAL SOCIETY
Article
pubs.acs.org/JACS

High Thermoelectric and Reversible *p-n-p* Conduction Type Switching Integrated in Dimetal Chalcogenide

Chong Xiao,[†] Xinming Qin,[§] Jie Zhang,[‡] Ran An,[‡] Jie Xu,[†] Kun Li,[†] Boxiao Cao,[†] Jinlong Yang,*[,§] Bangjiao Ye,[‡] and Yi Xie*[,†]

[†]Division of Nanomaterials and Nanochemistry, Hefei National Laboratory for Physical Sciences at the Microscale, University of Science & Technology of China, Hefei, Anhui, 230026, P. R. China

[‡]Department of Modern Physics, University of Science & Technology of China, Hefei, Anhui, 230026, P. R. China

[§]Division of Theoretical and Computational Sciences, Hefei National Laboratory for Physical Sciences at the Microscale, University of Science & Technology of China, Hefei, Anhui, 230026, P. R. China

Supporting Information

ABSTRACT: The subject of the involved phase transition in solid materials has formed not only the basis of materials technology but also the central issue of solid-state chemistry for centuries. The ability to design and control the required changes in physical properties within phase transition becomes key prerequisite for the modern functionalized materials. Herein, we have experimentally achieved the high thermoelectric performance (ZT value reaches 1.5 at 700 K) and reversible *p-n-p* semiconducting switching integrated in a dimetal chalcogenide, $AgBiSe_2$ during the continuous hexagonal−rhombohedral−cubic phase transition. The clear-cut evidences in temperature-dependent positron annihilation and Raman spectra confirmed that the *p-n-p* switching is derived from the bimetal atoms exchange within phase transition, whereas the full disordering of bimetal atoms after the bimetal exchange results in the high thermoelectric performance. The combination of *p-n-p* switching and high thermoelectric performance enables the dimetal chalcogenides perfect candidates for novel multifunctional electronic devices. The discovery of bimetal atoms exchange during the phase transition brings novel phenomena with unusual properties which definitely enrich solid-state chemistry and materials science.

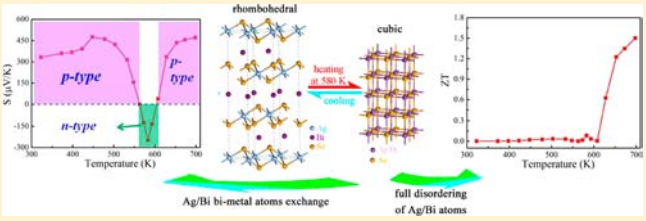

INTRODUCTION

Occurrence of transformation between different polymorphic phases is a common observed phenomenon in inorganic compounds, and the subject of phase transition in solid materials has grown continuously and enormously, forming not only the basis of materials technology but also the central issue of solid-state chemistry for centuries, thanks to both the ability to alter the properties of solid materials and the fundamental understanding of the crystallographic features.[1,2] Besides such phase transitions involving changes in atomic configuration, solids also undergo transformations where the electronic or the spin configuration changes, which should unexpectedly bring novel physical properties of solids, such as superconductor,[3,4] superionic conductor,[5] giant magnetocaloric,[6] optical storage,[7] and so on. So, the ability to design and control the required changes in physical properties within phase transition becomes key prerequisite for the modern functionalized materials. Although several theories have been put forward to explain the varied characteristics of polytypism, a challenge faces us in our quest for an in-depth and full comprehensive understanding of the crystallography of phase transformations, such as that the atoms exchange during the phase transition brings unusual properties is rarely reported.

As one of the most important inorganic solid-state materials, due to their ability to direct conversion of heat into electricity, thermoelectric generators are today well recognized as viable renewable-energy sources and a very promising candidate to aid in the worldwide energy crisis.[8] The performance of thermoelectric materials is quantified by a dimensionless figure of merit, ZT, which is defined as $\sigma \cdot S^2 T/(\kappa_l + \kappa_e)$, where σ is the electrical conductivity, S is the Seebeck coefficient, T is the absolute temperature, κ_l is the lattice thermal conductivity, and κ_e is the carrier thermal conductivity. According to the Wiedemann−Franz law, only the lattice thermal conductivity, κ_l, is independent of the electrical conductivity.[9] Therefore, progress in enhancing the ZT values by substantial reduction of lattice thermal conductivity is highly desirable.[10,11]

A more modern strategy in the search for high ZT thermoelectric materials is associated with the development and primary evaluation of new theoretical concepts, of which the Slack idea of "phonon-glass electron-crystal" (PGEC) has been of the greatest importance.[12] PGEC materials would idealistically behave as a glass with respect to phonon scattering (low thermal conductivity) and as a crystal with respect to

Received: September 8, 2012
Published: October 15, 2012

dx.doi.org/10.1021/ja308936b | J. Am. Chem. Soc. 2012, 134, 18460−18466

electron scattering (high electrical conductivity). The development of the PGEC concept gave rise to new ideas in the preparation of thermoelectric materials with low thermal conductivity based on the narrow-gap semiconductor. In fact, semiconductors are modern key materials offering manifold perspectives for the increasing electronic devices, which depend on their conduction type. However, their intrinsic thermal conductivity is still usually high because of the long phonon mean free path in a periodic structure, and furthermore, the reduction of thermal conductivity can only be limited to the so-called "alloy limit".[13] Fortunately, the disordered narrow-gap semiconductors provide a promising candidate for the PGEC concept,[14] because they possess both high electrical conductivity and low thermal conductivity because of the ions disordering in the crystalline lattice, such as those chalcogenides compounds, which show high thermoelectric performance in the disordering state.[15−17]

On the other hand, it is interesting that the majority of disordered semiconductors undergo the reversible order−disorder transition as the temperature is varied, usually accompanying with significant change of electrical and/or thermal properties. Recently, we have reported the order−disorder transition (induced by semiconductor-superionic conductor phase transition) in silver chalcogenides nanocrystals could be an effective way to selectively optimize the thermoelectric power factor based on the modulation of the electric transport property across the phase transition.[18] And this intriguing property accompanied with phase transition has attracted more attention for the construction of intelligent devices.[19,20]

Dimetal chalcogenide, $AgBiSe_2$, as a typical polymorphous semiconductor,[21,22] showing a very intriguing phase behavior, structural variability and high degree of Ag/Bi bimetal ions disordering in the high temperature lattice, especially the bimetal atoms exchange during the phase transition, may exhibit more sophisticated and unexpected electrical/thermal transport than that in binary silver chalcogenides.

Taking the above two views into consideration, in this current study, we proposed a new concept that dimetal chalcogenides may show more sophisticated and unexpected properties due to the potential bimetal atoms exchange during the phase transition, and for the first time, we have experimentally achieved the high thermoelectric performance and reversible *p-n-p* semiconducting switching integrated in a dimetal chalcogenide, $AgBiSe_2$ during the continuous hexagonal-rhombohedral-cubic phase transition. That is, the *p-n-p* conduction switching and high thermoelectric properties integrated in a unique solid. The ZT value of our $AgBiSe_2$ nanocrystals reaches 1.5 at 700 K, which is a very high value and comparable to the best of the novel bulk thermoelectric materials, thanks to the full disordering of Ag/Bi atoms in high temperature cubic lattice. The Ag−Bi atoms exchange during the phase transition enables $AgBiSe_2$ reversibly switch between *p*- and *n*-type conduction.

EXPERIMENTAL SECTION

Materials. All chemicals were of analytic grade purity obtained from Sinopharm Chemical Reagent Co., Ltd., and used as received without further purification.

Synthesis of $AgBiSe_2$ Nanocrystals. $AgBiSe_2$ nanocrystals were synthesized through a simple colloidal method. Briefly, slurry of bismuth(III) citrate (0.199 g) in 20 mL of oleylamine was heated at 120 °C for 30 min under an N_2 atmosphere to remove oxygen and water. The solution was then heated to 180 °C under vigorous magnetic stirred, and 0.085 g of $AgNO_3$ was quickly added at this temperature. After the mixture was magnetically stirred for 10 min, 0.079 g selenium powder was quickly added into the system. The mixture was maintained at 180 °C for 3 h under magnetic stirred. After the resulting solution was cooled to room temperature, the nanocrystals were separated from the resulting solution by centrifuge and washed for several times with ethanol and cyclohexane. All the samples were dried in a vacuum at 60 °C for 6 h.

Characterization. Temperature-dependent XRD (X-ray diffraction) patterns of the samples were recorded between 27 and 330 °C by the Shimadzu XRD-7000 with Cu Kα radiation (λ = 1.54187 Å). X-ray photoelectron spectroscopy (XPS) measurements were performed on a VGESCALAB MK II X-ray photoelectron spectrometer with an excitation source of Mg Kα = 1253.6 eV. Electron microscopy observations were carried out with a Hitachi H-800 transmission electron microscope at 100 kV. High-resolution transmission electron microscopy (HRTEM) images were performed on JEOL-2010 transmission electron microscope at 200 kV. Thermal gravimetric analysis (TGA) of the as synthesized samples was carried out on a NETZSCH TG 209 F3 thermal analyzer from room temperature to 400 °C with a heating rate of 5 °C min^{-1} in N_2. Differential scanning calorimetry (DSC) cycling curves were measured by the NETZSCH DSC Q2000 with a heating/cooling rate of 5 °C min^{-1} between 20 and 400 °C. Temperature-dependent Raman spectra were recorded between 20 and 387 °C with a LABRAM-HR Confocal Laser MicroRaman Spectrometer 750 K with a laser power of 0.5 mW.

Thermoelectric Property Measurements. The possibly residual organic surfactants were removed via the procedure of previous report[23] before fabrication of bulk samples for thermoelectric measurement. Briefly, as-prepared $AgBiSe_2$ nanocrystals were dispersed in cyclohexane with hydrazine solution (85% v/v) and stirring vigorously until all the nanocrystals are precipitated. The supernatant is decanted and the precipitate is washed with ethanol for three times to remove hydrazine and collected by centrifugation, and then dried in vacuum at 65 °C. After the hydrazine treatment, the nanocrystals are hot-pressed into rectangular (10 mm ×4 mm ×1.5 mm) and round disk bulk smaples (with diameter of about 13 mm and thickness of 2 mm) under 60 MPa at 300 °C for 30 min. Rectangular shape samples were employed to simultaneously measure electrical conductivity σ and Seebeck coefficient S by the standard four-probe methods in a He atmosphere (ULVAC-RIKO ZEM-3). Thermal conductivity κ was calculated using the equation $\kappa = a\rho C_p$ from the thermal diffusivity obtained by a flash diffusivity method (LFA 457, Netzsch) on the round disk sample, specific heat C_p determined by a differential scanning calorimeter method (DSC Q2000, Netzsch).

Positron Annihilation Spectroscopy. The positron lifetime experiments were carried out with a fast-slow coincidence ORTEC system with a time resolution of about 230 ps full width at half-maximum. A 5mCi source of ^{22}Na was sandwiched between two identical samples, and the total count was one million. The temperature-dependent Doppler broadening energy spectroscopic (DBES) spectra were measured using an HP Ge detector at a counting rate of approximately 800 cps. The energy resolution of the solid-state detector was 1.5 keV at 0.511 MeV (corresponding to positron 2γ annihilation peak). The total number of counts for each DBES spectrum at different temperature was 8 million. Because of the high temperature, the Hp Ge detector should be put a little far away from the sample and the ^{22}Na source was dropped on a Nickel membrane. Considering the problem of counting rate, the positron single Doppler broadening experiment was adopted.

Calculations. The structural optimization, total energies and electronic structure calculations were performed by using VASP code[24] with the projector-augmented wave (PAW) potentials.[25] Generalized gradient (GGA) corrections were applied to the exchange-correlation function within the implementation of Perdew, Burke, and Ernzerhof (PBE).[26] After the full convergence test, the kinetic energy cutoff of the plane wave basis was chosen to be 450 eV. The Brillouin zone of hexagonal unit cell and cubic supercell are sampled in the k-space within the Monkhorst−Pack scheme[27] by (15 × 15 × 3) and (4 × 4 ×

dx.doi.org/10.1021/ja308936b | J. Am. Chem. Soc. 2012, 134, 18460−18466

4) mesh points for the self-consistent structure optimizations, (21 × 21 × 5) and (5 × 5 × 5) mesh points for the total energy calculations, respectively. All atomic positions and lattice parameters are optimized by using the conjugate gradient method where total energy and atomic forces are minimized. The convergence for energy is chosen as 10^{-5} eV between two ionic steps, and the maximum force allowed on each atom is 0.01 eV/Å. The band decomposed charge density is obtained by summing up the local density of states for the eigenvalues at a specified band, which is provided to analyze the orbital characters near Fermi surface, including VBM and CBM in the semiconductor. The 3D charge density isosurfaces have been drawn by VESTA.[28]

RESULTS AND DISCUSSION

$AgBiSe_2$, as a typical member of I−V−VI_2 compounds with phase transition behavior, its temperature-dependent structural evolution is well-known as shown in Figure 1a. At room

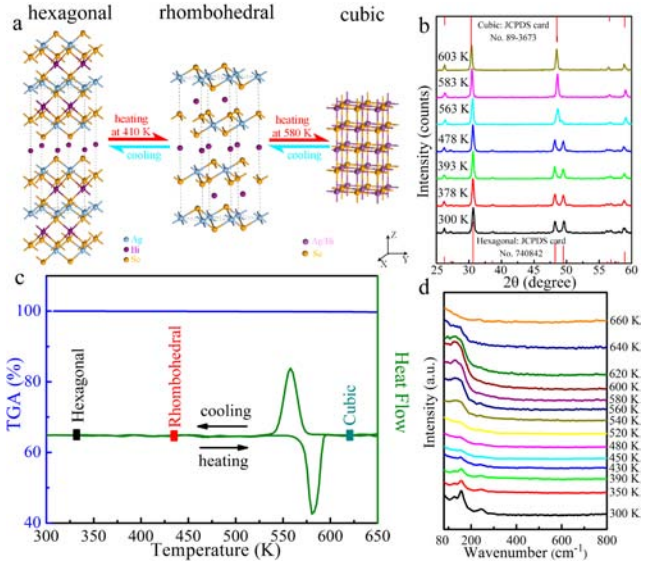

Figure 1. (a) Crystal structural evolution among hexagonal, rhombohedral, and cubic phase. (b) Temperature-dependent XRD patterns for $AgBiSe_2$ nanocrystals. (c) TGA and DSC curves for $AgBiSe_2$ nanocrystals. No obvious mass loss was detected in the whole temperature, while a broad endothermic was observed between 555 and 595 K. (d) Temperature-dependent Raman spectra for $AgBiSe_2$ nanocrystals.

temperature, $AgBiSe_2$ is a *p*-type semiconductor and crystallizes in the hexagonal phase with parameters a = 4.18 Å and c = 19.67 Å (space group $P\bar{3}m1$). As temperature increases, $AgBiSe_2$ is observed to undergo continuous phase transition to rhombohedral phase around 410 K and then to cubic phase around 580 K. This reversible phase transition will undergo from a high-temperature cubic phase to an intermediate-temperature rhombohedral structure around around 560 K and then to a low-temperature hexagonal phase around 393 K as temperature decreases.[21,22] In the intermediate temperature rhombohedral phase (space group $R\bar{3}m$ with lattice constants a = 7.022 Å and α = 34.5°), ordering of Ag and Bi atoms takes place in quite distinguishable positions, while in the high temperature cubic phase (space group $Fm\bar{3}m$ with lattice constants a = 5.832 Å), the Ag and Bi atoms are fully disordering. Inspired by the structural analysis, $AgBiSe_2$ nanocrystals were synthesized through a simple colloidal method for the first time. X-ray diffractograms from synthetic $AgBiSe_2$ nanocrystals (Figure 1**b**) exhibit peaks corresponding to the hexagonal structure with space group of $P\bar{3}m1$[see JCPDS files #74−0842]. No extraneous peaks are observed, indicating that the samples consist of pure phase. The calculated lattice parameters a = 4.16 Å and c = 19.68 Å agree with JCPDS values. Temperature-dependent XRD patterns (Figure 1b) clearly show the structural transition from the rhombohedral to the cubic phase. While the hexagonal-rhombohedral phase transition was not differentiated in the temperature-dependent XRD patterns, which prove that atoms slightly shift rather than rearrange during this phase transition. This is consistent with the DSC result (Figure 1c). The appearance of endothermic and exothermal peaks in DSC curves during the heating and cooling process clearly confirms the fully reversible phase transition of $AgBiSe_2$. Thermal analysis (Figure 1c) externalizes the hexagonal-rhombohedral phase transition without showing drastic volume changes, which is responsive to the slightly atoms shift in the lattice during this phase transition. Meanwhile, the reversible rhombohedral-cubic phase transition is observed around 580 K featuring a broad endothermic response over the temperature range 555 K < T < 595 K, consistent with temperature-dependent XRD results. In fact, since hexagonal-rhombohedral phase transition process only involves the slight movement of atoms, hexagonal and rhombohedral phase of $AgBiSe_2$ exhibit almost the same XRD diffraction patterns (see in Supporting Information Figure S1). However, the clear-cut evidence in temperature-dependent Raman spectra (Figure 1d) also confirmed that our originally synthetic sample is hexagonal $AgBiSe_2$: apparent Raman spectra variations were observed during the phase transition, and the details will be discussed later.

Transmission electron microscopy (TEM, Figure 2a) experiments confirmed that our synthetic products are hexagonal phase $AgBiSe_2$ nanoparticles with size around 10 nm at room temperature. The HRTEM images (Figure 2b) of one individual nanocrystal indicated the distances between the

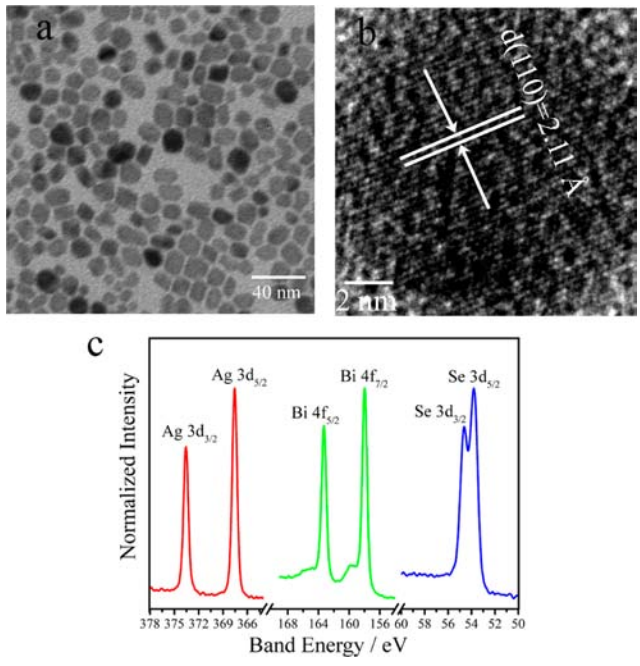

Figure 2. (a) TEM and (b) HRTEM image of $AgBiSe_2$ nanocrystals. (c) XPS spectra of the synthetic $AgBiSe_2$ nanocrystals.

dx.doi.org/10.1021/ja308936b | J. Am. Chem. Soc. 2012, 134, 18460−18466

adjacent lattice fringes to be 2.11 Å, which corresponds to the lattice spacing of the (1 1 0) *d*-spacing for orthorhombic $AgBiSe_2$ (2.09 Å, JCPDS 74−0842). X-ray photoelectron spectroscopy (XPS, Figure 2c) was used to characterize the composition of as-prepared $AgBiSe_2$ nanocrystals. The binding energies of Ag $3d_{3/2}$ and Ag $3d_{5/2}$ for $AgBiSe_2$ located at 373.6 and 367.5 eV with a peak splitting of 6.1 eV, which was consistent with the standard reference XPS spectrum of Ag (I). The two strong peaks at 157.9 and 163.3 eV can be attributed to Bi $4f_{7/2}$ and Bi $4f_{5/2}$, respectively. The peaks at 53.8 and 54.6 eV can be assigned to the Se $3d_{5/2}$ and Se $3d_{3/2}$ respectively. Taking into account the atomic sensitivity factors of Ag, Bi and Se, the atomic ratio of Ag/Bi/Se is approximately 1:1:2 according to quantification of the peak areas of Ag 3d, Bi 4f and Se 3d. No peaks of other elements are observed in the wide XPS survey spectrum, indicating the high purity of the $AgBiSe_2$ product.

The thermoelectric properties of our $AgBiSe_2$ nanocrystals samples were measured and shown in Figure 3. As shown in

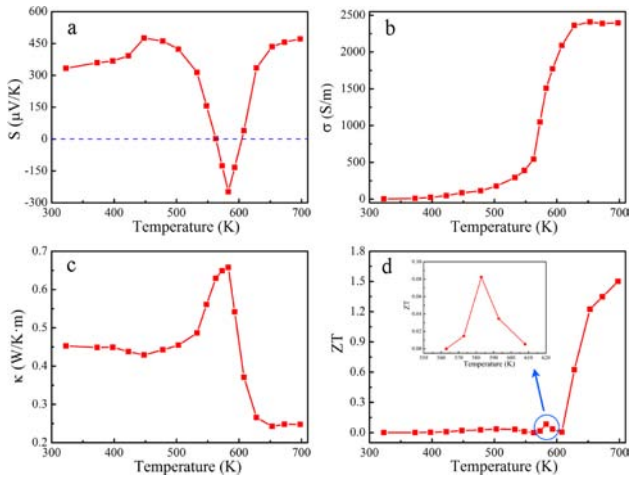

Figure 3. Temperature dependences of Seebeck coefficient *S* (a), electrical conductivity σ (b), thermal conductivity κ (c), and dimensionless figure-of-merit ZT (d). A pronounced peak in the Seebeck coefficient with two changes in the sign of the value was observed. This feature is consistent with the substantial entropy component found during DSC. A rapid increase of ZT value with the increasing temperature was observed, which reached 1.5 around 700 K.

Figure 3a, the positive Seebeck coefficient values at low temperature are indicative of *p*-type semiconductor of hexagonal $AgBiSe_2$, and as temperature increases, the Seebeck coefficient slightly increases from 390 μV/K to 460 μV/K around 423 K, which is the hexagonal-rhombohedral phase transition temperature. As temperature further increases, during the rhombohedral to cubic phase transition, the Seebeck coefficient changes sign from 480 μV/K to −250 μV/K and then changes back to 470 μV/K. As the negative sign of the Seebeck coefficient is indicative of *n*-type conduction, $AgBiSe_2$ obviously manifests the unusually reversible *p-n-p* switching within the broad rhombohedral-cubic phase transition range observed by temperature-dependent XRD and DSC curves.

The temperature-dependent electrical and thermal conductivity of $AgBiSe_2$ nanocrystals are presented in Figure 3b and c, respectively. Pronounced increase in electrical conductivity and decrease in thermal conductivity with temperature increasing to near 583 K also clearly reflect the typical phase transition behavior. It is well-known that when $AgBiSe_2$ crystallizes in cubic phase at high temperature, Ag and Bi ions distribute statistically between the close packed layers of selenium ions in NaCl-type lattice, resulting in the high electrical conductivity because of the high mobility of these disordering ions.[22] At the same time, the Ag/Bi disordering could cause much stronger anharmonicity of the chemical bond, which drives the phonon−phonon umklapp scattering intrinsically limit the lattice thermal conductivity.[29]

The ZT values of our $AgBiSe_2$ nanocrystals are calculated as shown in Figure 3d. Thanks to the high electrical conductivity and ultralow thermal conductivity which are derived from the Ag/Bi disordering in the lattice, the ZT value reaches 1.5 at 700 K, which is a very high value, and comparable to the best of the novel bulk thermoelectric materials.[30]

In additon to the high ZT value, which is derived from the fully disordering of Ag/Bi atoms in cubic lattice at high temperature, the Ag−Bi dimetal atoms exchange during the rhombohedral-cubic phase transition reveals another exciting phenomenon of reversible *p-n-p* switching. To investigate the source of this temperature dependent *p-n-p* switching, the origin of conduction type of hexagonal $AgBiSe_2$ should be first clarified since it has long been neglected, despite some previous reports accounted that the presence of Ag vacancies attributed to the *p*-type conduction for cubic phase of $I-V-VI_2$ compounds (such as $AgSbTe_2$).[31,32] Positron annihilation spectrometry is a well established technique to study the defects in solids, and the lifetime of the positron is able to give information about the type and relative concentration of defects/vacancies even at the ppm level.[33,34] The positron lifetime spectrum of our $AgBiSe_2$ nanocrystals yields two lifetime components, τ_1 (197.6 ps) and τ_2 (485 ps) with relative intensities I_1 (95.3%) and I_2 (4.7%) (Figure 4a). The longer component (τ_2) can be designed to the larger size defects in the material, while the shorter one (τ_1) belongs to Ag vacancies, which is obviously the overwhelming defect in the sample.

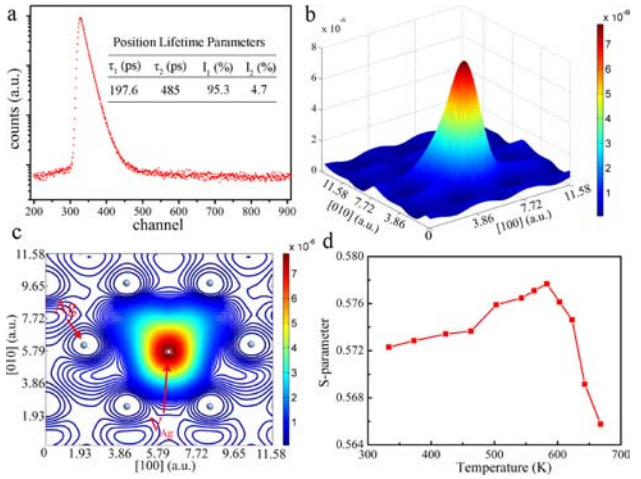

Figure 4. (a) Positron lifetime spectrum of $AgBiSe_2$ nanocrystals yield two lifetime components, which are designed to the Ag vacancies and larger size defects respectively. (b and c) Schematic representations of trapped positrons for $AgBiSe_2$ nanocrystals in basal plane and (001) plane. It is clearly seen that the positron is mostly trapped by negatively charged V_{Ag} (V_{Ag} denote Ag vacancy) in $AgBiSe_2$ nanocrystals. (d) Doppler broadening *S* parameter for $AgBiSe_2$ nanocrystals as a function of temperature. *S* parameter approaches a maximum value around 580 K indicating the most abundant valence electrons.

dx.doi.org/10.1021/ja308936b | J. Am. Chem. Soc. 2012, 134, 18460−18466

Figure 4b and c represent the projection of the calculated positron density distribution for the basal plane and (001) plane. It is shown that positrons are distributed around the Ag vacancies, which are the most negatively charged part. Furthermore, theoretical calculation also shows that the formation energy (E_f^v) of an Ag vacancy is the lowest among all other defects in this system, such as Bi vacancy, Se vacancy, and interstitial ions (Supporting Information Table S2). So, it is reasonably believed that the *p*-type conduction in hexagonal $AgBiSe_2$ should be derived from the Ag vacancies.

On the other hand, in dimetal chalcogenides, for the ultimate dual-metal ions fully disordered state achieved after order–disorder transition, metal ions exchange will be inevitable during this transition. In fact, another important role of vacancy defects is acting as a bridge of atoms exchange.[35] Thus, here, the dimetal atoms exchange through vacancies during the thermal disorder process can be expected, and in order to investigate the detailed structural change information during the phase transition, we have performed temperature-dependent Raman scattering spectroscopy, which has been used extensively to study the lattice vibrations,[36,37] and Figure 1d clearly exhibited the obvious Raman peak change during the phase transition. Structural analysis and theoretical calculations (details see in Supporting Information Figure S2–S4) revealed that, in hexagonal $AgBiSe_2$ lattice, the atomic arrangement can be considered as repeating units with each consisting of eleven atomic Se–Ag–Se–Bi–Se-Ag–Se–Bi–Se–Ag–Se chain (denoted as Ag–Bi–Se chain) along the *c* axis, which is then separated by a layer of Bi. Obviously, two crystallographically distinct Bi atoms are observed in this structure: Bi2 is bonded to Se atoms with distance of 2.993 and 2.981 Å, whereas Bi1 is isolatedly inserted to two Ag–Bi–Se layers and weakly bonded with Se atoms with distance of 3.04 Å. While in the rhombohedral phase, the Bi2–Se bonds are weakened and all Bi atoms locate at the same chemical environment. It is known that the Bi–Se bonds show 4 Raman-active modes in Bi_2Se_3, consisted of Se–Bi–Se–Bi-Se quintuple layers.[38] In Figure 1d, the Raman peaks at 124 cm^{-1} and 157 cm^{-1} can also be assigned to E_g^2 and A_{1g}^2 mode of Bi–Se bonds, respectively. As temperature increases, the Bi2–Se bonds are weakened in rhombohedral phase (Figure 5), therefore the two characteristic Raman peaks disappear. With temperature further increasing, the rhombohedral phase begins the transformation to cubic phase, the Ag–Bi atoms exchange through Ag vacancies should take place during the phase transition, which can also be verified by Raman spectroscopy: there reappear the two characteristic Raman peaks which appear in hexagonal phase, indicating the reappearance of Bi–Se bonds during the rhombohedral-cubic phase transition. When $AgBiSe_2$ completely transforms into cubic phase, Ag/Bi are in full disordering in lattice, so the macroscopic polarizability disappears, and no Raman peaks are observed again.

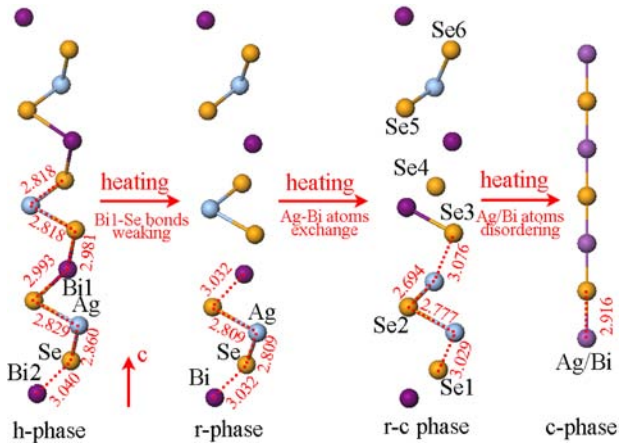

Figure 5. Schematic representations of the atomic rearrangement for Ag–Bi–Se chain during the phase transition.

Moreover, a typical phonon softening behavior has been observed during the rhombohedral-cubic phase transition, that is, Raman peaks shift downward and exhibit obvious widening. This phonon softening in narrow-gap semiconductor during the thermal disorder has been confirmed to be usually accompanied with the closing of the gap and increasing in the density at the Fermi level.[39] Band structure calculations show that $AgBiSe_2$ in both hexagonal and rhombohedral phase with Ag vacancies is *p*-type semiconductor, while a quasi-metallic state occurs during the rhombohedral-cubic phase transition shown in Figure 6a and e. Band-decomposed partial charge densities (Figure 6b, c, and d) show that the valence bands and the conduction bands of rhombohedral phase $AgBiSe_2$ are formed predominantly by Ag *d*-states (hybridized with Se *p*-states) and Bi *p*-states (hybridized with Se *p*-states), respectively. While, after exchange between Ag and Bi atom, half-filled bands across Fermi level occurs, which are predominantly distributed at the Ag atoms of Ag–Se–Ag chains (Figure 6f and g). This electronic band structure changes during the rhombohedral-cubic phase transition have also been confirmed by PDOS analysis and the results are presented in Figure 7. As shown in Figure 7, after exchange between Ag and Bi, it is clearly that the *p* states of Se, especially Se2, drop down and below the Fermi level where the *d* states of Ag1 and Ag2 go opposite. Furthermore, the *p* states of Bi1 and Bi2 are also seen to drop down slightly in energy. From partial charge density analysis, these half-filled bands across Fermi level mainly originate from the Ag–Se–Ag chains, which result in the quasi-metallic state. Consequently, it can be concluded that the formation of the Ag–Se–Ag chains based on the Ag–Bi atoms exchange results in continuous electronic bands distributed in the chains to form an intermediate quasi-metallic state, in which valence electron conduction increases.

Furthermore, the unique *p-n-p* switching can also be confirmed by Doppler broadening of the annihilation radiation, which is an effective technique to reflect momentum distribution of the annihilating electrons,[40] and the results are analyzed in terms of the so-called *S* parameter, which is defined as the area under the central part of the annihilation photopeak divided by the total area. Since the vacancy-type defects act as trapping sites for positrons, and thus annihilation with low energy valence electrons at these defects results in a narrowing of the photopeak corresponding to an increase in the *S* parameter.[41] In the present case, we carried out the temperature-dependent Doppler broadening and the *S* parameter is shown in Figure 4d. It is clearly seen that during the rhombohedral to cubic phase transition, the *S* parameter increases to a maximum around 580 K, implying the most abundant valence electrons, which is also consistent with the band structure calculation. As $AgBiSe_2$ transforms into cubic phase, the Ag/Bi atoms are full disordering in lattice, and the conduction type of $AgBiSe_2$ changes back to *p*-type conduction due to the presence of Ag vacancies.

dx.doi.org/10.1021/ja308936b | J. Am. Chem. Soc. 2012, 134, 18460–18466

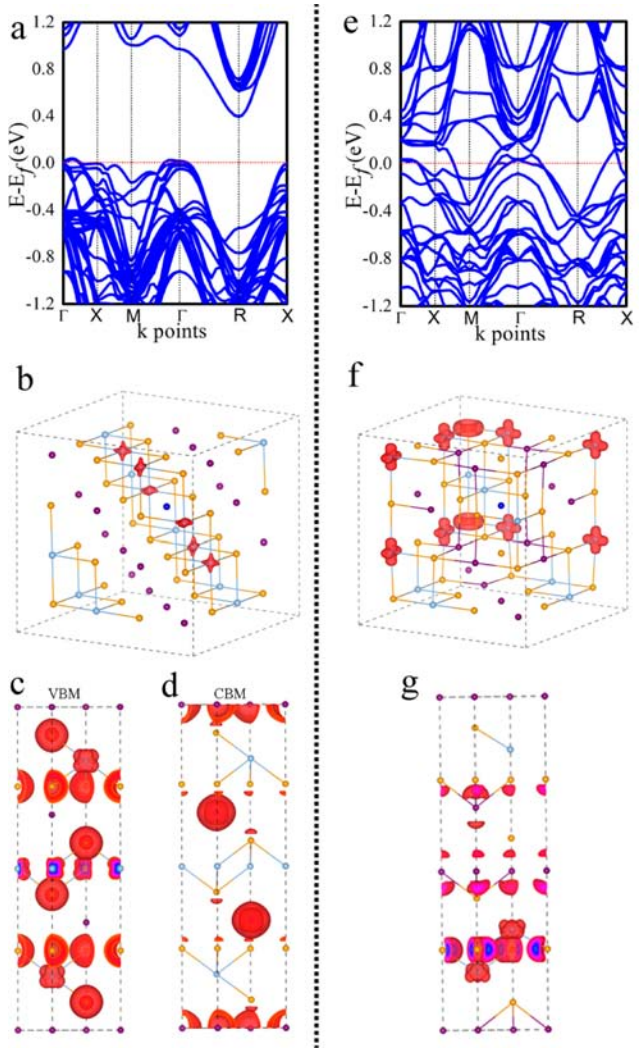

Figure 6. Band structure and band-decomposed charge density plots for rhombohedral (a, b) and intermediate (e, f) phase $AgBiSe_2$, respectively. Partial charge density plots for (c) the VBM (valence band maximum) and (d) the CBM (conduction band minimum) of Ag−Bi−Se chain in the rhombohedral phase $AgBiSe_2$. (g) The partial charge density plots of Ag−Bi−Se chain for $AgBiSe_2$ after the Ag/Bi atoms exchange during the rhombohedral-cubic phase transition.

In fact, the reversible *p-n-p* conduction type switching was first reported in $Ag_{10}Te_4Br_3$,[19] in which the weakening of the bonds and the reorganization of the Te_4 entity result in a reorganization of the electronic bands with an intermediate quasi-metallic state. Compared to the $Ag_{10}Te_4Br_3$, the obvious difference in this study is the characteristic of dimetal ions in dimetal chalcogenides $AgBiSe_2$. During the rhombohedral-cubic phase transition, the Ag/Bi bimetal exchange through the Ag vacancies in the Ag−Bi−Ag chain, brings the change of the DOS at the Fermi level and the following quasi-metallic states, as a result, a clear *p-n-p* switching was observed in $AgBiSe_2$.

CONCLUSIONS

In summary, we proposed a new concept that dimetal chalcogenides may show more sophisticated and unexpected properties because of the potential bimetal atoms exchange during the phase transition, and for the first time, we have experimentally achieved the high thermoelectric performance and reversible *p-n-p* semiconducting switching integrated in a

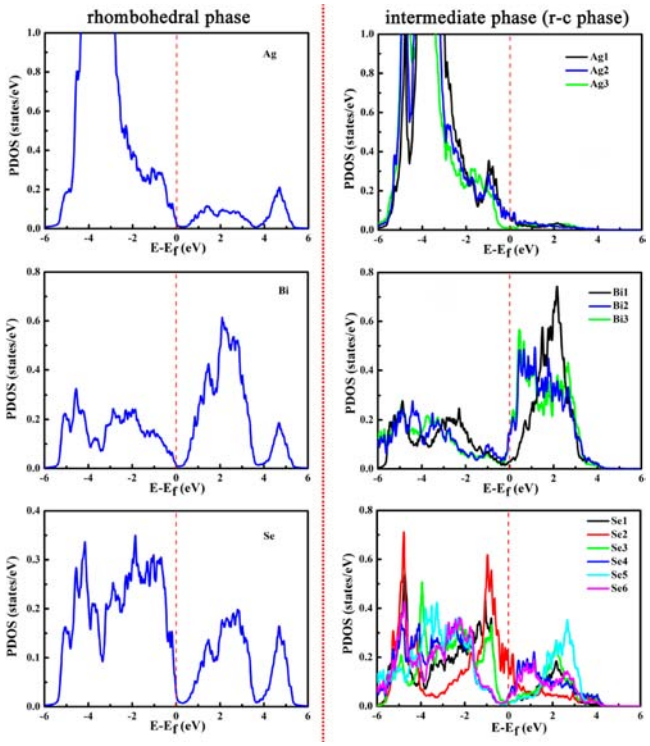

Figure 7. Projected density of states (PDOS) for rhombohedral (left column) and intermediate (right column) phase of $AgBiSe_2$ during the rhombohedral-cubic phase transition.

dimetal chalcogenide, $AgBiSe_2$ during the continuous hexagonal-rhombohedral-cubic phase transition. The insights gained from the experimental results and theoretical calculations in this study indicate that the Ag−Bi atoms exchange during the rhombohedral-cubic phase transition plays an important role in the *p-n-p* switching. During the thermal disorder process, Ag−Bi atoms exchange results in a quasi-metallic state bringing more conduction valence electrons, which eventually lead to the switching between *p*- and *n*-type conduction. In addition, further full disordering of Ag/Bi in lattice at high temperature causes much stronger anharmonicity of the chemical bond and drives the phonon−phonon umklapp, as a result, scattering could intrinsically limit the lattice thermal conductivity, and simultaneously show high electrical conductivity due to the high mobility of these disordering ions. Consequently, high ZT value of 1.5 was obtained around 700 K, which is comparable to the best of the novel bulk thermoelectric materials. Our finding revealed that dimetal chalcogenides semiconductors not only may be a unique catalog of material both for temperature dependent *p-n-p* switching and high performance thermoelectric devices, and open a new avenue to design multifunctional materials and device. The discovery of bimetal atoms exchange during the phase transition brings novel phenomena with unusual properties which definitely enrich solid-state chemistry and materials science.

ASSOCIATED CONTENT

Supporting Information

Detailed calculations for $AgBiSe_2$. This material is available free of charge via the Internet at http://pubs.acs.org.

dx.doi.org/10.1021/ja308936b | J. Am. Chem. Soc. 2012, 134, 18460−18466

AUTHOR INFORMATION

Corresponding Author

E-mail: yxie@ustc.edu.cn (Y.X.); jlyang@ustc.edu.cn (J.Y.).

Notes

The authors declare no competing financial interest.

ACKNOWLEDGMENTS

This work was financially supported by National Basic Research Program of China (No. 2009CB939901, 2011CB921404), National Natural Science Foundation of China (11079004, 90922016, 10979047, J1030412, 21121003), innovation project of Chinese Academy of Science (KJCX2-YW-H2O).

REFERENCES

(1) Zhang, M. X.; Kelly, P. M. *Prog. Mater. Sci.* **2009**, *54*, 1101.
(2) Rao, C. N. R. *Acc. Chem. Res.* **1984**, *17*, 83.
(3) Kasahara, S.; Shi, H. J.; Hashimoto, K.; Tonegawa, S.; Mizukami, Y.; Shibauchi, T.; Sugimoto, K.; Fukuda, T.; Terashima, T.; Nevidomskyy, A. H.; Matsuda, Y. *Nature* **2012**, *486*, 382.
(4) Coronado, E.; Marti-Gastaldo, C.; Navarro-Moratalla, E.; Ribera, A.; Blundell, S. J.; Baker, P. J. *Nat. Chem.* **2010**, *2*, 1031.
(5) Makiura, R.; Yonemura, T.; Yamada, T.; Yamauchi, M.; Ikeda, R.; Kitagawa, H.; Kato, K.; Kakata, M. *Nat. Mater.* **2009**, *8*, 476.
(6) Liu, J.; Gottschall, T.; Skokov, K. P.; Moore, J. D.; Gutfleisch, O. G. *Nat. Mater.* **2012**, *11*, 620.
(7) Ohkoshi, S.-I.; Tsunobuchi, Y.; Matsuda, T.; Hashimoto, K.; Namai, A.; Hakoe, F.; Tokoro, H. *Nat. Chem* **2010**, *2*, 539.
(8) Bell, L. E. *Science* **2008**, *321*, 1457−1461.
(9) Kanatzidis, M. G. In *Semiconductors and Semimetals*; Terry, M. T., Ed.; Elsevier: Amsterdam, 2001; Vol. *69*, p 5.
(10) Pernot, G.; Stoffel, M.; Savic, I.; Pezzoli, F.; Chen, P. *Nat. Mater.* **2010**, *9*, 491−495.
(11) Wan, C. L.; Wang, Y. F.; Wang, N.; Norimatsu, W.; Kusunoki, M.; Koumoto, K. *Sci. Technol. Adv. Mater.* **2010**, *11*, 044306.
(12) Slack, G. A. In *CRC Handbook of Thermoelectrics*; Rowe, D. M., Ed.; CRC: Boca Raton, FL, 1995; pp 407−440.
(13) Vineis, C. J.; Shakouri, A.; Majumdar, A.; Kanatzidis, M. G. *Adv. Mater.* **2010**, *22*, 3970.
(14) Snyder, G. J.; Christensen, M.; Nishibor, E.; Caillat, T.; Iversen, B. B. *Nat. Mater.* **2004**, *3*, 458.
(15) Xiao, C.; Xu, J.; Cao, B. X.; Li, K.; Kong, M. G.; Xie, Y. *J. Am. Chem. Soc.* **2012**, *134*, 7971.
(16) Zaikina, J. V.; Kovnir, K. A.; Sobolev, A. N.; Presniakov, I. A.; Kytin, V. G.; Kulbachinskii, V. A.; Olenev, A. V.; Lebedev, O. L.; Tendeloo, G. V.; Dikarev, E. V.; Shevelkov, A. V. *Chem. Mater.* **2008**, *20*, 2476.
(17) Liu, H. L.; Shi, X.; Xu, F. F.; Zhang, L. L.; Zhang, W. Q.; Chen, L. D.; Li, Q.; Uher, T.; Snyder, G. J. *Nat. Mater.* **2012**, *11*, 422.
(18) Xiao, C.; Xu, J.; Li, K.; Feng, J.; Yang, J. L.; Xie, Y. *J. Am. Chem. Soc.* **2012**, *134*, 4287.
(19) Nilges, T.; Lange, S.; Bawohl, M.; Deckwart, J. M.; Janssen, M.; Wiemhofer, H. D.; Decourt, R.; Chevalier, B.; Vannahme, J.; Eckert, H.; Weihrich, R. *Nat. Mater.* **2009**, *8*, 101.
(20) Wu, C. Z.; Wei, H.; Ning, B; Xie, Y. *Adv. Mater.* **2010**, *22*, 1972.
(21) Manolikas, C.; Spyridelis, J. *Mater. Res. Bull.* **1977**, *12*, 907.
(22) Larson, P.; Mahanti, S. D. Presented at the American Physical Society, Annual March Meeting, March 12−16, 2001.
(23) Scheele, M.; Kornowski, A.; Klinke, C.; Weller, H. *Adv. Funct. Mater.* **2009**, *19*, 3476−3483.
(24) Kresse, G.; Hafner, J. *Phys. Rev. B* **1993**, *47*, R558.
(25) Blöchl, P. E. *Phys. Rev. B 1994* **1994**, *50*, 17953.
(26) Perdew, J. P.; Burke, K.; Ernzerhof, M. *Phys. Rev. Lett.* **1996**, *77*, 3865.
(27) Monkhorst, H. J.; Pack, J. D. *Phys. Rev. B* **1976**, *13*, 5188.
(28) Momma, K.; Izumi, F. *J. Appl. Crystallogr.* **2011**, *44*, 1272 ; code available from http://jp-minerals.org/vesta/en/.
(29) Morelli, D. T.; Jovovic, V.; Heremans, J. P. *Phys. Rev. Lett.* **2008**, *101*, 035901.
(30) Snyder, G. J.; Toberer, E. S. *Nat. Mater.* **2008**, *7*, 105.
(31) Ye, L. H.; Hoang, K.; Freeman, A. J.; Mahanti, S. D.; He, J.; Tritt, T. M.; Kanatzidis, M. G. *Phys. Rev. B* **2008**, *77*, 245203.
(32) Jovovic, V.; Heremans, J. P. *Phys. Rev. B* **2008**, *77*, 245204.
(33) Chakraverty, S.; Mitra, S.; Mandal, K.; Nambissan, P. M. G.; Chattopadhyay, S. *Phys. Rev. B* **2005**, *71*, 024115.
(34) Sun, W.; Li, Y. Z.; Shi, W. Q; Zhao, X. J.; Fang, P. F. *J. Mater. Chem.* **2011**, *21*, 9263.
(35) Yin, Y. D.; Rioux, R. M.; Erdonmez, C. K.; Hughes, S.; Somorjai, G. A.; Alivisatos, A. P. *Science* **2004**, *304*, 711.
(36) Polking, M. J.; Urban, J. J.; Milliron, D. J.; Zheng, H. M.; Chan, E.; Caldwell, M. A.; Raoux, S.; Kisielowski, C. F.; Ager, J. W.; Ramesh, R.; Alivisatos, A. P. *Nano Lett.* **2011**, *11*, 1147.
(37) Panchal, V.; Lopez-Moreno, S.; Santamaria-Perez, D.; Errandonea, D.; Manjon, F. J.; Rodriguez-Hernandez, P.; Munoz, A.; Achary, S. N.; Tyagi, A. K. *Phys. Rev. B* **2011**, *84*, 024111.
(38) Zhang, J.; Peng, Z. P.; Soni, A.; Zhao, Y. Y.; Xiong, Y.; Peng, B.; Wang., J. B.; Dresselhaus, M. S.; Xiong, Q. H. *Nano Lett.* **2011**, *11*, 2407−2414.
(39) Delairea, O.; Marty, K.; Stone, M. B.; Kent, P. R.; Lucas, M. S.; Abernathy, D. L.; Mandrus, D.; Sales, B. C. *Proc. Natl. Acad. Sci. U.S.A.* **2011**, *108*, 4725.
(40) Wu, Y. C.; Kallis, A.; Jiang, J.; Coleman, P. G. *Phys. Rev. Lett.* **2010**, *105*, 066103.
(41) Rummukainen, M.; Makkonen, I.; Ranki, V.; Puska, M. J.; Saarinen., K. *Phys. Rev. Lett.* **2005**, *94*, 165501.